Efficiency Penalty Analysis for Pure H_2 Production Processes with CO_2 Capture

Wei Feng, Peijun Ji, and Tianwei Tan
College of Life Science and Technology and College of Chemical Technology,
Beijing University of Chemical Technology, Beijing, 100029, China

DOI 10.1002/aic.11052
Published online November 20, 2006 in Wiley InterScience (www.interscience.wiley.com).

The conventional steam-reforming (CSR) process is a major process for the production of pure hydrogen from natural gas with CO_2 as the main by-product. In this work, based on the CSR process, several alternative H_2-producing processes with CO_2 capture are simulated and analyzed. The alternative processes capture the CO_2 by concentrating the CO_2 through the approaches including burning some of the separated H_2 instead of CH_4 in the furnace, using pure oxygen instead of air for the combustion of fuel gas, applying a prereformer to reduce the usage of pure oxygen, and applying an H_2-membrane in the steam reformer to separate pure H_2. The reactors of the CSR process and the alternative processes with CO_2 capture were simulated based on the kinetic models of the reactions. The CSR process and the alternative processes were evaluated in terms of the thermodynamic efficiency, the amount of high pressure (HP) H_2 produced per mole of CH_4, the amount of CO_2 produced per mole of HP H_2, and the CO_2 captured per mol of HP H_2. The efficiency penalties for CO_2 capture of the alternative processes were compared and discussed. *AIChE J*, 53: 249–261, 2007
Keywords: steam reforming, H_2 membrane, CO_2 capture, simulation, thermodynamic efficiency

Introduction

In the foreseeable future, natural gas will continue to be generally regarded and preferred as the major feedstock for the manufacture of hydrogen.[1,2] CO_2 capture and storage have been recognized as a necessity with the growing concerns with respect to global warming.[3,4] For the capture of carbon dioxide, it is not sufficient to consider only the amount of CO_2 captured because the CO_2-capture process itself costs energy. For example, an efficiency drop of 9% results from the CO_2 capture with an amine absorption/desorption unit at a gas-fired combined cycle.[4] The recovery of CO_2 is largely hindered by the dilution of the CO_2 with nitrogen.[4]

Correspondence concerning this article should be addressed to P. Ji at Jipj@mail.buct.edu.cn.

For CO_2 capture, reducing the efficiency penalties of various capture technologies is very important. In this work, we evaluate the CO_2 capture based on steam-reforming processes producing hydrogen from natural gas. The conventional steam-reforming (CSR) process without CO_2 capture, which is the major process for converting natural gas to H_2, is taken as the basis process and other steam-reforming processes considering CO_2 capture as the alternative ones. The reactors of the processes are simulated and analyzed based on the kinetic models of the reactions available in the literature and the simulation results provide a solid basis for the analysis. The CSR process and the alternative processes are evaluated in terms of the thermodynamic efficiency, the amounts of high pressure (HP) H_2 produced per mole of CH_4, the amounts of CO_2 produced per mole of HP H_2, and the amounts of CO_2 captured. The dual objectives of this work are (1) to determine how the efficiency penalties for CO_2 capture can be reduced more effectively and (2) to give some suggestions on the future development of H_2 production process with CO_2 capture in consideration.

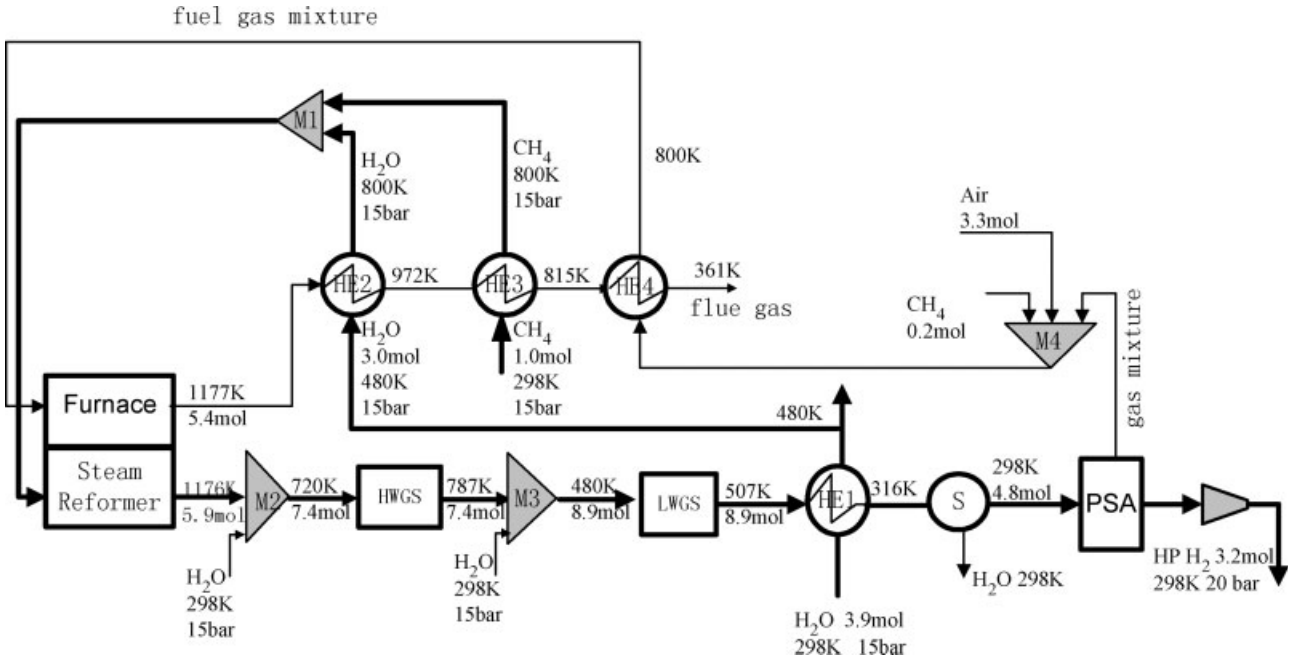

Figure 1. Scheme of the CSR process without CO_2 capture (Process 1).

HE: heat exchanger; M: mixer; S: separator.

Process Description

The conventional steam-reforming process without CO_2 capture (Process 1)

The scheme of the CSR process without CO_2 capture is shown in Figure 1. Through a conventional steam reformer (SR), methane is converted by steam-reforming reaction to syngas, which is a mixture of hydrogen, carbon monoxide, and carbon dioxide. To decrease the temperature and increase the ratio of H_2O to CO, water is mixed with syngas in the mixers (M2 and M3), after which the syngas is introduced into the high-temperature water-gas-shift (HWGS) and low-temperature water-gas-shift (LWGS) converters, by which most of the CO in the syngas is converted to H_2. The temperature of the stream from LWGS is adjusted to the operation temperature of pressure swing adsorption (PSA) through a heat exchanger HE1. Through the unit of PSA, 70–85% of the total H_2 produced can be recovered as pure hydrogen.[5] Heat recovery is considered in Process 1; for example, the rejected gas mixture from the PSA is mixed with some fresh methane and air in the mixer M4, after which the gas mixture is introduced into the furnace of the steam reformer; the inlet CH_4 and steam of the steam reformer are preheated in the heat exchangers HE2 and HE3 by heat exchanging with the flue gas from the furnace.

The CSR process with pure O_2 input (Process 2)

Process 2 is shown in Figure 2. Similar to Process 1, Process 2 also includes a conventional steam reformer, HWGS and LWGS converters, and heat exchangers. The heat exchangers are used for heat recovery and preheating the inlet reactants for the conventional steam reformer. Process 2 also considers the reuse of the rejected fuel gas mixture by feeding it to the furnace together with some fresh CH_4. In contrast to Process 1, Process 2 introduces pure O_2 instead of air for the combustion of fuel gas in the furnace and the combustion of methane in the heater. In this way the CO_2 in the flue gas can be captured directly after the separation of water. The highly concentrated CO_2 is then compressed to 20 bar as a product of high-pressure (HP) CO_2.

The CSR process with hydrogen combusted (Process 3)

As shown in Figure 3, Process 3 has the same operation units as described for Process 2. However, in Process 3, some of the pure hydrogen produced instead of methane is burned in the heater to heat up the fresh methane (as a reactant) and in the furnace to provide the heat required by the steam-reforming reaction. In Process 3, pure O_2 instead of air is used both in the furnace and in the heater to avoid dilution of the CO_2 by nitrogen. After separating water from the flue gas, the CO_2 is highly concentrated and then compressed as HP CO_2.

The CSR process with a prereformer (Process 4)

The scheme of Process 4 is shown in Figure 4. Compared to Process 1, Process 4 includes a prereformer, whereas the other operation units such as HWGS and LWGS converters, heat exchangers, and PSA have the same functions as described for Process 1. In the unit of the prereformer, the rejected fuel gas mixture from the PSA together with pure O_2 are introduced into Furnace A to provide heat for the reforming reaction, and thus dilution of CO_2 is avoided. Through the prereformer, the methane is partly converted and the generated gas mixture containing CH_4, H_2, CO_2, and CO is then introduced into the steam reformer, where CH_4 is further converted. In Furnace B, some pure H_2 from the PSA is burned with air to provide the heat required by the steam reforming

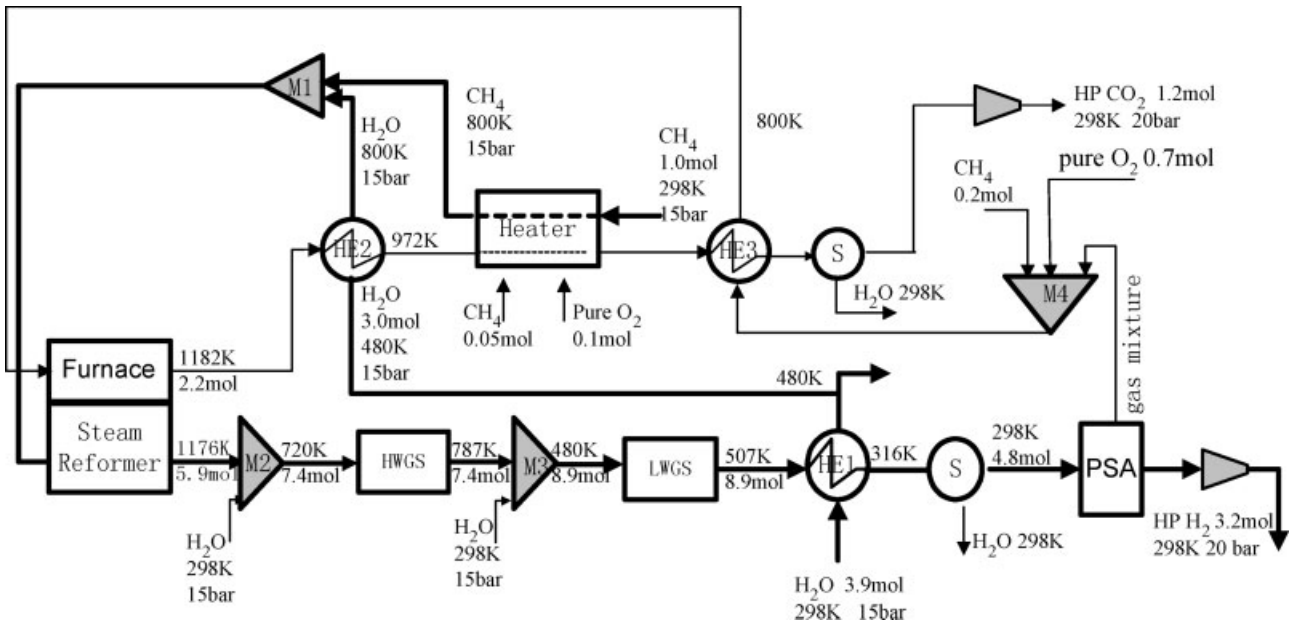

Figure 2. Scheme of the CSR process with pure O_2 input (Process 2).

HE: heat exchanger; M: mixer; S: separator.

of CH_4. In Furnace B, pure H_2 is burned and no CO_2 is produced. Because of feeding pure O_2, Furnace A releases highly concentrated CO_2, which can be compressed as the product of HP CO_2.

The H_2 membrane steam-reforming (MSR) process without CO_2 capture (Process 5)

Process 5 (Figure 5) is a process with an H_2-membrane steam reformer. The hydrogen formed in the H_2-membrane steam reformer is separated out through the H_2-membrane when the reactions take place. The removal of hydrogen can promote the conversion of methane. Because the H_2-membrane steam reformer combines the functions of producing and separating H_2 together, Process 5 does not need water-gas-shift converters and the PSA unit. Therefore, Process 5 is much more simplified compared to the pure H_2 production processes with a conventional steam reformer. In the H_2-membrane steam reformer, because the permeation of H_2 is driven by the difference in the H_2 partial pressure, to maintain a

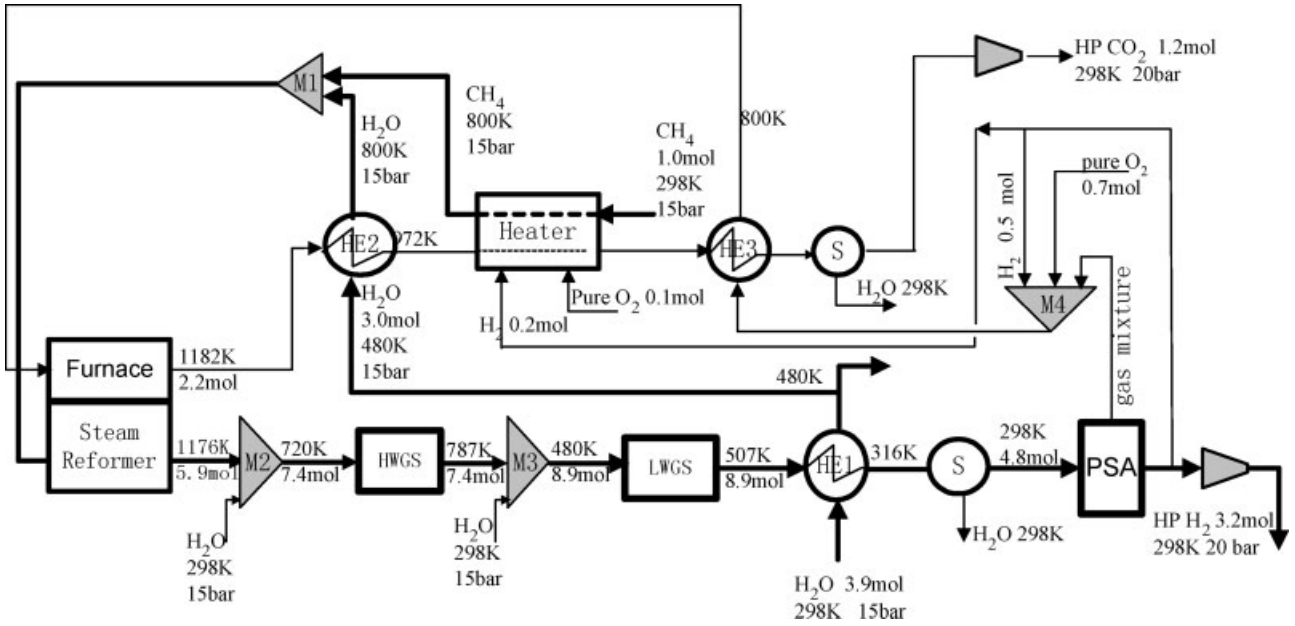

Figure 3. Scheme of the CSR process with an H_2 fired furnace (Process 3).

HE: heat exchanger; M: mixer; S: separator.

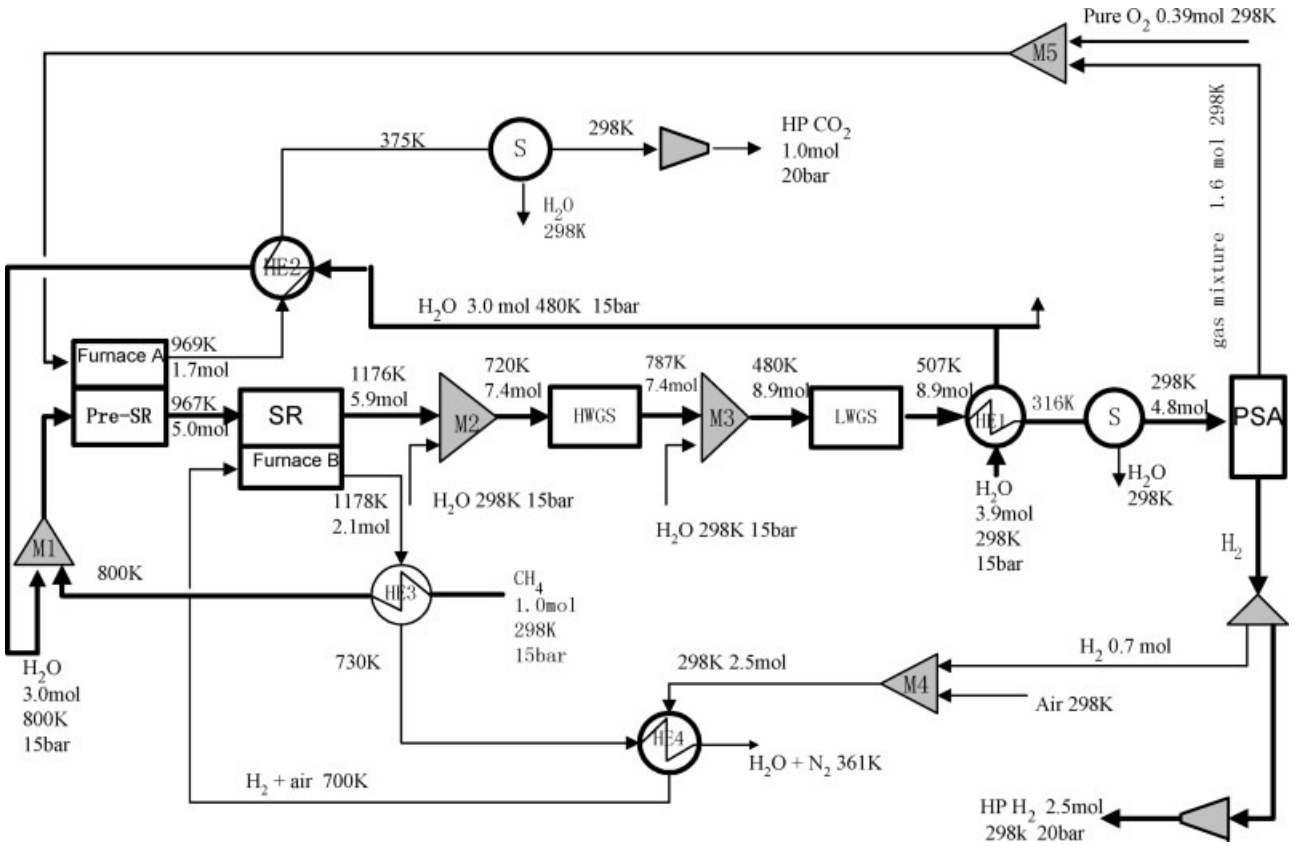

Figure 4. Scheme of the CSR process with a prereformer (Process 4).

HE: heat exchanger; M: mixer; S: separator.

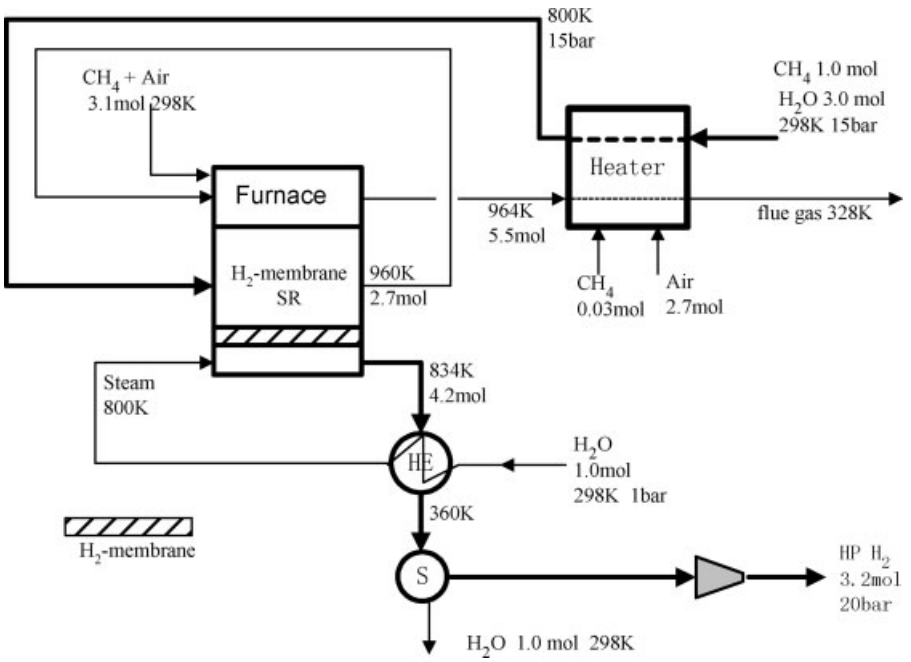

Figure 5. The scheme of the H_2 MSR process without CO_2 capture (Process 5).

HE: heat exchanger; S: separator.

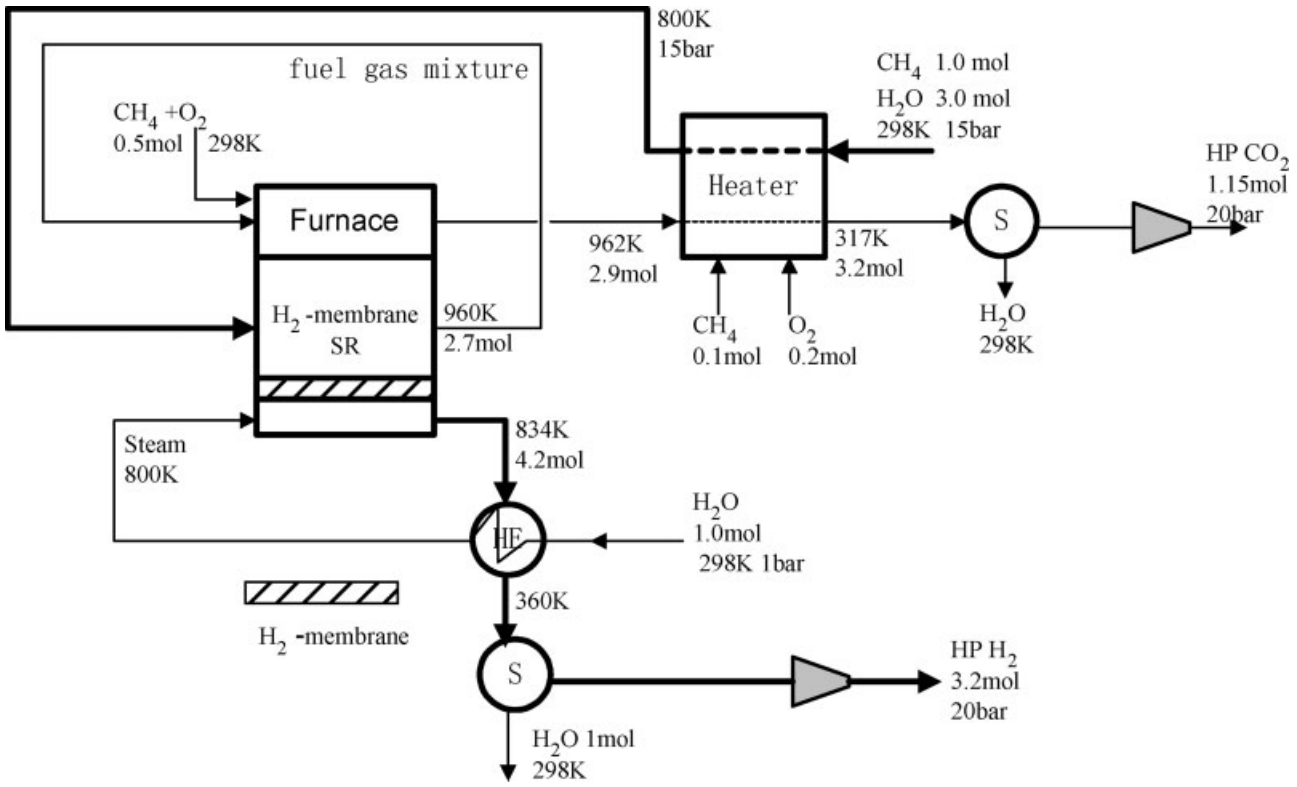

Figure 6. Scheme of the H_2 MSR process with pure O_2 input (Process 6).

HE: heat exchanger; S: separator.

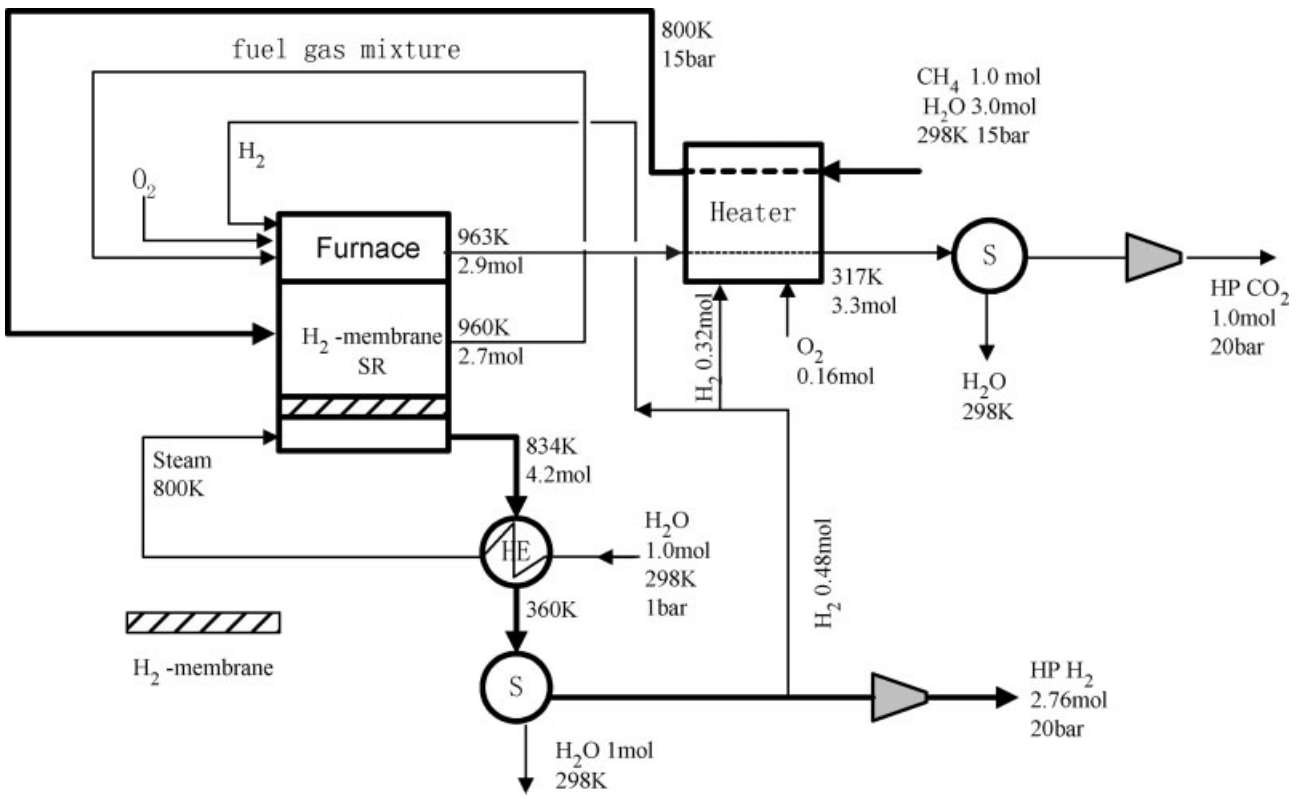

Figure 7. Scheme of the H_2 MSR process with an H_2 fired furnace (Process 7).

HE: heat exchanger; S: separator.

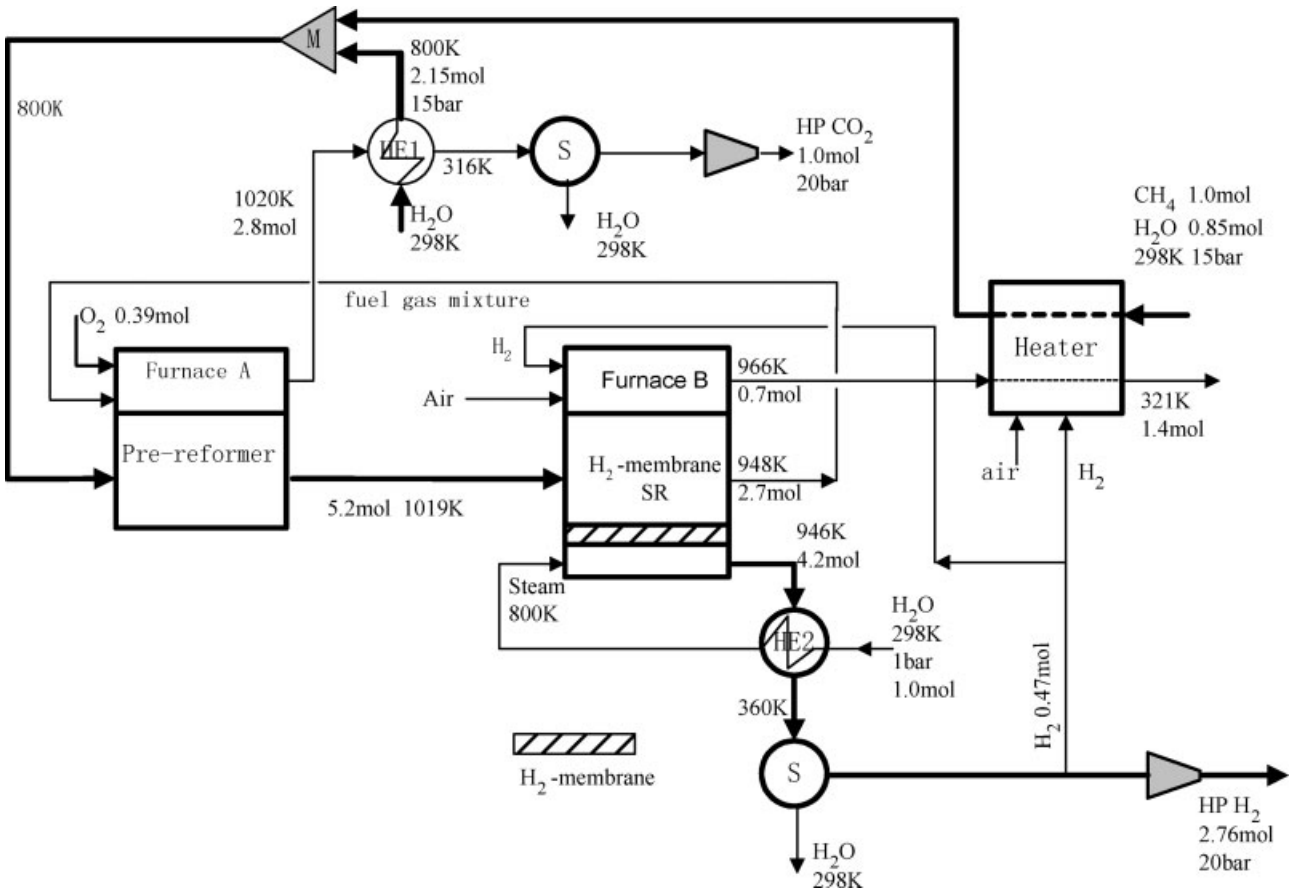

Figure 8. Scheme of the H_2 MSR process with a prereformer (Process 8).

HE: heat exchanger; S: separator.

lower partial pressure in the permeate side, steam is used as the sweeping gas.

For heat recovery, heat exchangers are used to heat up the reactants or the sweeping gas. Together with some fresh methane, the fuel gas mixture containing unconverted CH_4, CO, and unseparated H_2 from the reformer is reused. In the furnace and the heater, the fuel gas mixture is combusted with air. The CO_2 produced by Process 5 is not captured because of the low concentration of CO_2 in the flue gas.

The H_2 MSR process with pure O_2 input (Process 6)

Similar to Process 5, Process 6 (Figure 6) is a process with an H_2-membrane steam reformer. Compared to Process 5, Process 6 considers the CO_2 capture by introducing pure O_2 instead of air into the furnace and heater. The heat recovery is accomplished through heat exchanging and reuse of the rejected fuel gas mixture from the H_2-membrane steam reformer. After separating water from the flue gas, the highly concentrated CO_2 is obtained and compressed to 20 bar as the product of HP-CO_2.

The H_2 MSR process with an H_2-fired furnace (Process 7)

With a process structure similar to that of Process 5, Process 7 (Figure 7) makes use of part of the pure hydrogen produced for the combustion with pure O_2 in the furnace and in the heater. The heat exchangers have the same function as that in processes 5 and 6. The rejected fuel gas mixture from the H_2-membrane steam reformer is reused in the furnace. Because of the use of pure O_2 for the combustion, the flue gas contains highly concentrated CO_2 after the water separation, and then the CO_2 is compressed to 20 bar as HP CO_2.

The H_2 MSR process with a prereformer (Process 8)

As shown in Figure 8, Process 8 contains a prereformer and an H_2-membrane steam reformer. Methane is partly converted in the prereformer and further (more completely) converted in the H_2-membrane steam reformer. The rejected gas mixture from the H_2-membrane steam reformer, containing unconverted CH_4, CO, and unseparated H_2, is fed into Furnace A to combust with pure O_2. In Furnace B and the heater, part of the pure H_2 produced is burned with air to provide the heat required by the steam-reforming reaction or to heat up the reactants. Because H_2 is combusted with pure O_2, the flue gas from Furnace B and the heater do not contain CO_2. Because of the feeding of pure O_2, Furnace A releases highly concentrated CO_2 (after condensing water), which is then compressed as HP CO_2.

Table 1. Reaction Rate for the Reactions in the Steam Reformers

Reaction	Kinetics of Reaction
1) $CH_4 + H_2O \Longleftrightarrow CO + 3H_2$	$R_1 = \frac{(k_1/p_{H_2}^{2.5})(p_{CH_4}p_{H_2O} - p_{H_2}^3 p_{CO}/K_{eq1})}{DEN^2}$
2) $CO + H_2O \Longleftrightarrow CO_2 + H_2$	$R_2 = \frac{(k_2/p_{H_2})(p_{CO}p_{H_2O} - p_{H_2}p_{CO_2}/K_{eq2})}{DEN^2}$
3) $CH_4 + 2H_2O \Longleftrightarrow CO_2 + 4H_2$	$R_3 = \frac{(k_3/p_{H_2}^{3.5})(p_{CH_4}p_{H_2O}^2 - p_{H_2}^4 p_{CO_2}/K_{eq3})}{DEN^2}$

Note: $DEN = 1 + K_{CO}\,p_{CO} + K_{H_2}\,p_{H_2} + K_{CH_4}\,p_{CH_4} + K_{H_2O}\,p_{H_2O}/P_{H_2}$

Simulation Work

Definition of boundary conditions

For simulating the processes, the following boundary conditions are defined:

The CH_4 input into the processes is at 15 bar and 298 K; water and air input into the processes are at atmospheric conditions.

The pure H_2 produced and the CO_2 captured are compressed to 20 bar as product and by-product, respectively.

For the conventional SR and the H_2-membrane SR, the inlet temperature, the inlet pressure, and the inlet ratio of steam to methane in the reaction side are 800 K, 15 bar, and 3:1, respectively.

For the steam reformer, no coke deposition is assumed.[6]

For the H_2-membrane SR, the pressure of the permeate side is set to 1 bar.

The pressure drop of the gas mixture along the processes is neglected.

Methane conversion of 95% is set for the conventional SR and the H_2-membrane SR.

The inlet temperatures of the HWGS and LWGS reactors are set to 720 and 480 K, respectively.

Electricity is assumed to be produced from CH_4 with a thermodynamic efficiency of 50%.[7]

20% of heat loss is assumed in the heat exchangers.

Simulation of the steam reformers

Kinetic Models for Steam Reforming of Methane. For the steam reforming of methane over a nickel-supported catalyst, Xu and Froment[8] suggested two main reactions for methane steam reforming together with a water-gas-shift reaction, and they developed the corresponding kinetic rate equations, which are listed in Table1. The kinetic models developed by Xu and Froment have been widely adopted for the simulation of this process.[9]

The kinetics of the steam-reforming reactions to CO and CO_2 and the kinetics of the water-gas-shift reaction suggested by Xu and Froment are also adopted for the simulation of the steam reformers in this work. Both the rate equations and the kinetic parameters needed in the calculations of the reaction rate are summarized in Tables 1–3.

Table 2. Parameter Values for the Expression $k_k = k_k^0 \exp(-E_{a,k}/RT)$ for the Reaction Rate Constant

Reaction	k_k^0 [mol/($kg_{cal} \cdot s$)]	$E_{a,k}$ (J/mol)
1) k_1	1.17×10^{15} bar$^{0.5}$	240.1×10^3
2) k_2	5.43×10^5 bar^{-1}	67.13×10^3
3) k_3	2.83×10^{14} bar$^{0.5}$	243.9×10^3

Table 3. Parameters for the Expression $K_i = K_i^0 \exp(-\Delta H_{ads,i}/RT)$ for the Adsorption Coefficients

Adsorption Coefficient	K_i^0	$\Delta H_{ads,i}$ (kJ/mol)
K_{CH_4}	6.65×10^{-4} bar^{-1}	−38.28
K_{CO}	8.23×10^{-5} bar^{-1}	−70.65
K_{H_2}	6.12×10^{-9} bar^{-1}	−82.90
K_{H_2O}	1.77×10^5	88.68

Simulation Models for the Conventional Steam Reformer and the Prereformer. For the simulation of the conventional steam reformer and the prereformer, a one-dimensional steady-state heterogeneous model is adopted. The transport mechanism in the axial direction is considered to be of the plug-flow type. The influence of intraparticle concentration gradients within the catalyst pellet is taken into account by solving the solid-phase continuity equation at each increment along the fixed bed reactor coordinate. The gas-phase continuity equation, energy equation, and solid-phase continuity equation are presented in Table 4; the corresponding inlet and boundary conditions are also listed. In the reactor models, the subscript i represents the reaction gas species, that is, CH_4, H_2O, CO, H_2, and CO_2. U_1 [227 J/($m^2 \cdot s \cdot K$)] represents the total heat transfer coefficient between the reaction region and the furnace in the steam reformer.[10] The temperature of the furnace is assumed to be constant along the reactor's axial coordinate.[11]

In the solid-phase continuity equation, the effective diffusivity of component i is related to the molecular and Knudsen diffusivities. The effective diffusivities are calculated according to the method in the literature.[12] The physical chemical properties Cp_i,[13] equilibrium constants,[14] and diffusivities[15] are considered to be temperature dependent. For a multicomponent mixture,

Table 4. Simulation Models for the Conventional Steam Reformer and the Prereformer

Gas-phase continuity equation

$$\frac{dF_i}{dz} = \sum_{k=1}^{N_R} \eta_k \upsilon_{ik} R_k (1 - \varepsilon_B) \rho_s^{SR} a_r$$

Gas-phase energy equation

$$\frac{dT_r^{SR}}{dz} = \frac{\rho_s^{SR}(1-\varepsilon_B)a_r \sum_k^{N_R}(-\Delta H_k \eta_k R_k) - q_{furnace}}{\sum_{i=1}^{5} F_i C_{Pi}}$$

$$q_{furnace} = U_1 a_w (T_r^{SR} - T_{Furnace}^{SR})$$

Solid-phase equations for calculating the effectiveness factors

$$\frac{1}{\xi^2}\frac{d}{d\xi}\left(D_{e,i}\xi^2 \frac{dp_{s,i}}{d\xi}\right) = 10^{-5} RT \rho_s^{SR} r_s^2 \sum_{k=1}^{N_R}(\upsilon_{ik} R_{s,k})$$

$$a_v \frac{D_{e,i}}{r_s}\frac{dp_{s,i}}{d\xi}\bigg|_{\xi=1} = 10^{-5} RT \sum_{k=1}^{N_R}(\eta_k \upsilon_{ik} R_k)$$

Solid-phase boundary conditions

$$\xi = 0, \frac{dp_{s,i}}{d\xi} = 0$$

Gas-phase boundary conditions

$$z = 0, \quad F_i = F_i|_{z=0}, \quad T = T_{in}$$

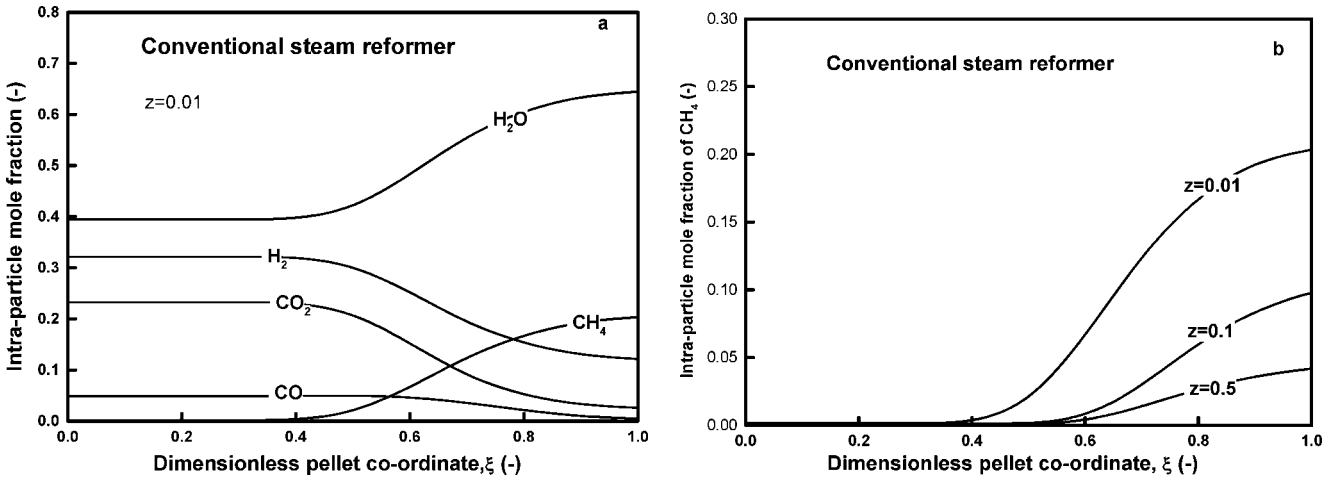

Figure 9. (a) Intraparticle mole fraction of reactant and product vs. dimensionless pellet coordinate, when the dimensionless reactor axial coordinate *z* at 0.01. (b) Intraparticle mole fractions of CH_4 vs. dimensionless pellet coordinate, when the dimensionless reactor axial coordinate *z* at 0.01, 0.1, and 0.5, respectively.

molecular diffusion is generally described by the Stefan–Maxwell approach. However, minor differences in concentration profiles calculated were observed between the Stefan–Maxwell approach and the binary diffusion approach.[16] Because of the small differences in diffusion coefficient of the different products and reactants, in this work, Fick's law is used to describe the molecular diffusion in the catalyst particle.

The model for a conventional steam reformer consists of a set of differential equations. The equations are solved at each increment of the axial reactor's coordinate. In each reactor increment, the solid-phase equation is solved first before the calculation of gas-phase equations. To solve the solid-phase equation, the pellet catalyst particle is normally divided into 10 to 20 shells. The number of shells needed depends on its effect on the final calculation results. For each shell, the steady-state differential solid-phase equation can be expressed in the form of difference equations represented by the intraparticle partial pressures of different species according to the mass balance of each shell. The mole change of each component caused by diffusion through the shell, $Diffusion|_{A_1} - Diffusion|_{A_2}$, is equal to the mole change caused by the reactions taking place inside the shell and is expressed as

$$D_{e.i}A_1\left|\frac{dp_{s.i}}{d\xi}\right|_{A_1} - D_{e.i}A_2\left|\frac{dp_{s.i}}{d\xi}\right|_{A_2} = 10^{-5}RTR_{S.K}\rho_s^{SR}dV \quad (1)$$

where A_1 and A_2 are areas.

Because of the partial pressure gradients of the species inside the catalyst particle, effectiveness factors have to be calculated and used to calculate actual reaction rates. The effectiveness factors for the reactions are calculated by

$$\eta_k = \frac{\int_0^v R_{S,K}\rho_s^{SR}dV}{R_K\rho_s^{SR}V} \quad (2)$$

Figure 9a shows the intraparticle mole fractions for both reactants and products as a function of the dimensionless pellet coordinate ξ, when the dimensionless reactor axial coordinate z is at 0.01. Figure 9b shows the intraparticle mole fractions of CH_4 as a function of dimensionless pellet coordinate, when the dimensionless reactor axial coordinate z is at 0.01, 0.1, and 0.5. As shown in Figure 9a, near the entrance of the reactor (z at 0.01), for both the reactants and the products, there are significant intraparticle mole-fraction gradients, when ξ is >0.4. With the increase of the reactor's axial coordinate, the gradient of intraparticle mole fraction of CH_4 becomes less pronounced as a result of consumption of the reactants and increase of the products, as indicated in Figure 9b. The calculated effectiveness factors are plotted as a function of the reactor's axial coordinate, as shown in Figure 10. For the two main reactions of methane steam reforming and the reaction of water-gas shift, the effectiveness factors decrease along the reactor's axial coordinate. The averaged effectiveness factors for the two main reactions of methane steam reforming are <0.1.

Simulation model for the H_2-membrane steam reformer

The equations of gas-phase continuity, energy, and solid-phase continuity of the reaction side as well as the continuity and energy equations of the nonreaction side for the H_2-mem-

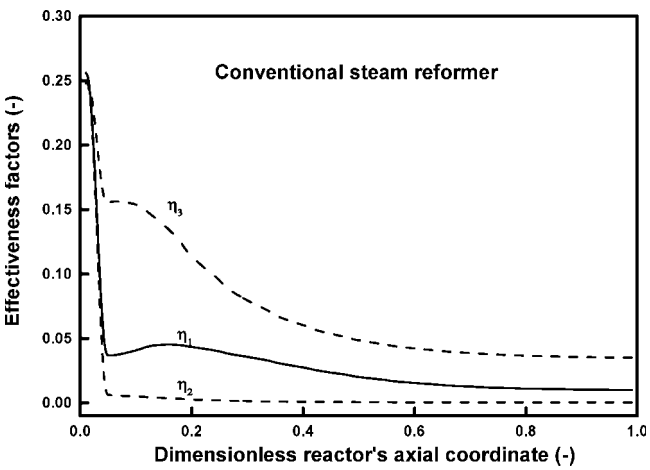

Figure 10. Effectiveness factors vs. dimensionless reactor axial coordinate for the conventional steam reformer.

Table 5. Simulation Models for the H_2-Membrane SR

Reaction side

Gas-phase continuity equation

$$\frac{dF_i}{dz} = \sum_{k=1}^{N_R} \eta_k \upsilon_{ik} R_k (1-\varepsilon_B)\rho_s^{SR} a_r - a_{H_2} N_i^{H_2}$$

$$N_4^{H_2} = N_{H_2}; \quad N_i^{H_2} = 0; \quad i \neq 4$$

Gas-phase energy equation

$$\frac{dT_r^{SR}}{dz} = \frac{1}{\sum_{i=1}^{5} F_i C_{Pi}} \left[\rho_s^{SR}(1-\varepsilon_B) a_r \sum_{k}^{N_R}(-\Delta H_k \eta_k R_k) - q_{furnace} - q_1\right]$$

$$q_{furnace} = a_w U_1 (T_r^{SR} - T_{Furnace}^{SR}); \quad q_1 = U_2 a_w (T_r^{SR} - T_{nr}^{SR})$$

Solid-phase equations for calculating the effectiveness factors

$$\frac{1}{\xi^2}\frac{d}{d\xi}\left(D_{e,i}\xi^2 \frac{dp_{s,i}}{d\xi}\right) = 10^{-5} RT \rho_s^{SR} r_s^2 \sum_{k=1}^{N_R}(\upsilon_{ik} R_{s,k})$$

$$a_v \frac{D_{e,i}}{r_s}\frac{dp_{s,i}}{d\xi}\Big|_{\xi=1} = 10^{-5} RT \sum_{k}^{N_R}(\eta_k \upsilon_{ik} R_k)$$

Nonreaction side

Continuity equation

$$\frac{dG_{H_2}}{dz} = a_{H_2} N_{H_2}$$

Energy equation

$$\frac{dT_{nr}^{SR}}{dz} = \frac{1}{\sum_j G_j C_{pj}}[q_1 + a_{H_2} N_{H_2} \Delta H_{H_2}]$$

Solid-phase boundary conditions

$$\xi = 0, \frac{dp_{s,i}}{d\xi} = 0$$

Gas-phase boundary conditions

$$z = 0, \quad F_i = F_i|_{z=0}, \quad T = T_{in}$$

brane steam reformer are presented in Table 5, in which the corresponding initial and boundary conditions are also listed. The energy equations take into account the heat of reaction, the heat exchanged between the nonreaction side (permeate side) and the reaction side, the heat exchanged between the furnace and the reaction side, and the energy carried by the diffusing of H_2. U_2 [2.4 J/(m^2·s·K)] represents the total heat transfer coefficient between the reaction region and the nonreaction side in the H_2-membrane SR.[10] Plug flow is assumed for both sides of the membrane. The temperature of the furnace is assumed to be constant along the reactor's axial coordinate.

The permeability of hydrogen through the H_2 permeable membrane is calculated according to the following equation:

$$N_{H_2} = \frac{P_m \exp\left(-\frac{E_A}{R\overline{T}}\right)}{\delta_{H_2}}\left(\sqrt{p_{H_2}^{high}} - \sqrt{p_{H_2}^{low}}\right) \quad (3)$$

The apparent activation energy E_A and the preexponential factor P_m of the membrane are 29.73 kJ/mol and 7.71 × 10^{-4} mol · m/(s · m^2·bar$^{0.5}$), respectively.[17]

In Eq. 3 $\overline{T}$ represents the operation temperature of the membranes, which is equal to the average temperature of the two sides of the membranes. $p_{H_2}^{high}$ and $p_{H_2}^{low}$ represent the higher and lower partial pressures of H_2 on the two sides of the membranes, respectively.

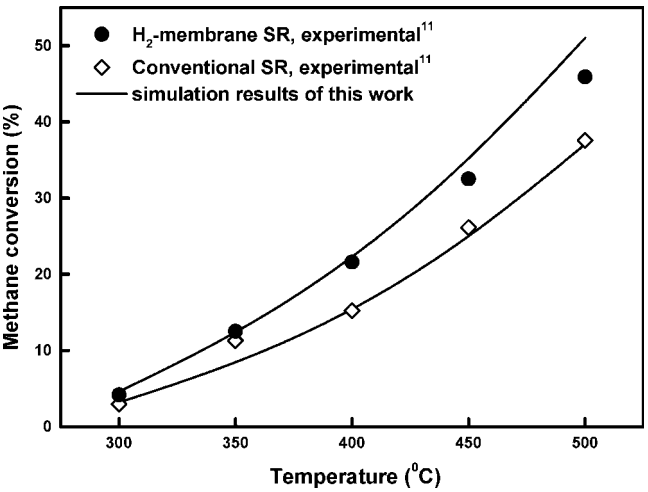

Figure 11. Comparison of the simulation results of this work with the experimental data of Shu et al.[11] in terms of methane conversions for the conventional SR and the H_2-membrane SR.

Validity of the Models for the Steam Reformers. The simulation results for the conventional steam reformer and the H_2-membrane steam reformer were compared with the experimental data from Shu et al.,[11] with very good agreement, as shown in Figure 11.

Simulation of the WGS reactors

Kinetic Models for the Water-Gas-Shift Reactions. For the water-gas-shift reactions converting CO into H_2 and CO_2, two classes of materials are used almost exclusively in industry as shift catalysts: the iron-based catalysts and the copper-based catalysts. The iron-based catalysts are the so-called high-temperature shift catalysts, operating from about 320 to 450°C. Copper-based shift catalysts have good activities at low temperatures with an operation range of about 200 to 250°C. Therefore copper-based shift catalysts are called low-temperature shift catalysts.

Bohlbro[18] found that the following empirical rate expression of Eq. 4 provided fairly good accuracy for the water-gas-shift reaction on an iron–chromium catalyst within the temperature range of 330 to 500°C and at atmospheric pressure:

$$-r_{CO}^{HWGS} = k^{HWGS}(p_{CO})^{0.90}(p_{H_2O})^{0.25}(p_{CO_2})^{-0.60}(1-\beta) \quad (4)$$

where $\beta = p_{CO_2}p_{H_2}/(p_{CO}p_{H_2O}K_{eq})$, $k^{HWGS} = k_0^{HWGS}\exp(-e_a/RT)$, $\ln k_0^{HWGS} = 16.68$, and $e_a = 114.6$ kJ/mol.

Table 6. Simulation Models for the High-Temperature Water-Gas-Shift (HWGS) and Low-Temperature Water-Gas-Shift (LWGS) Reactors

Continuity equation

$$\frac{dF_{CO}}{dz} = -a_r(1-\varepsilon_B)\rho_s^{WGS}(-r_{CO}^{WGS})$$

$$\frac{dF_{H_2}}{dz} = a_r(1-\varepsilon_B)\rho_s^{WGS}(-r_{CO}^{WGS})$$

Energy equation

$$\frac{dT^{WGS}}{dz} = \frac{1}{\sum F_i C_{Pi}}\Delta H_{WGS}\, a_r(1-\varepsilon_B)(-r_{CO}^{WGS})\rho_s^{WGS}$$

Table 7. Comparison of the Simulation Results with the Experimental Data for the HWGS Reactor*

	Feed Gas Composition (%)					Conversion (%)	
Feed (mol/h)	CO	CO_2	H_2	N_2	H_2O	Simulation	Experiment
2.279	50.7	0	0.38	22.9	26.0	7.1	7.0
2.254	48.4	0	0.37	4.4	46.8	8.3	8.0
2.317	47.6	0	0.36	18.4	33.6	7.4	7.6
2.296	50.2	0	0.38	42.7	6.7	5.6	5.4

*Adapted from Bohlbro.[18] Operation conditions: atmosphere; input temperature, 608 K; amount of catalyst, 3.00 g.

At elevated pressures, the same type of rate expression of Eq. 4 is valid: ln k increases in a linear fashion with ln P with a slope of 0.65.

For the simulation of low-temperature water-gas-shift (LWGS) reactors, the kinetic model of Amadeo[19] was used in this work, expressed in the following equation:

$$-r_{CO}^{LWGS} = \frac{0.92e^{-454.3/T} - p_{CO}p_{H_2O}(1-\beta)\cdot\psi}{(1 + 2.2e^{101.5/T}p_{CO} + 0.4e^{158.3/T}p_{H_2O} + 0.0047e^{2737.9/T}p_{CO_2} + 0.05e^{1596.1/T}p_{H_2})^2} \quad (5)$$

where ψ represents the effect of pressure: $\psi = 0.86 + 0.14P$ for $P \leq 24.8$ atm, and $\psi = 4.33$ for $P > 24.8$ atm.

Simulation Models for the WGS Reactors. The simulation models for the conventional HWGS reactor and LWGS reactor are specified in Table 6. Plug flow has been assumed in the reaction zone. The gas-phase continuity and energy equations and the initial and boundary conditions are listed in Table 6.

Validity of the Models for the WGS Reactors. The simulation results of the conventional HWGS and LWGS reactors were compared with the available experimental[18] or industrial data[20] in terms of the CO conversion or the exit gas composition, and very good agreement was attained. The comparison results are shown in Tables 7 and 8, respectively.

Simulation of the furnace and heater

The furnace and heater, which are used to provide energy for the steam-reforming reaction or heat up the reactants, are simulated by solving the following equation:

$$\frac{\Delta H_{heating}}{\eta_{fh}} + \Delta H\Big|_{T_{fg}}^{T_0} + \Delta H\Big|_{T_0}^{T_{end}} + \sum_{l=1}^{3} F_l^{fh}\Delta H_l^{com} = 0 \quad (6)$$

$\Delta H_{heating}$ represents the heat required to heat up the reactants or the energy required by the steam-reforming reactions. η_{fl} is the heating efficiency of the furnace or heater. F_l^{fh} and ΔH_l^{com} represent the molar flow rate and the heat from the combustion of the combustible component l, including CH_4, CO, and H_2, fed into the furnace at T_0, respectively. $\Delta H|_{T_0}^{T_{end}}$ represents the heat required to elevate the temperature of all after-combustion species (CO_2, H_2O, and N_2) from T_0 to T_{end}. T_{fg} represents the temperature of the gas mixture before being introduced into the furnace or the heater. $\Delta H|_{T_{fg}}^{T_0}$ is the heat released by the gas mixture when cooled down from T_{fg} to T_0.

Simulation of the compressors

The electric power needed by the compressors is calculated by assuming the thermodynamic efficiency of the compressor η_{cp} as 50%, using the following equation[21]:

$$W_{cp} = \frac{F_l RT_0}{\eta_{cp}} \ln\frac{P}{P_0} \quad (7)$$

Heat-exchanger simulation

Through energy balance, the heat exchangers are simulated with a heat loss of 20% assumed.

Some definitions for process simulation

In Processes 1, 2, 3, and 4, the ratio of H_2 recovery in the PSA is defined as

$$\sigma_R = \frac{F_{\text{pure } H_2}^{PSA}}{F_{H_2}^{PSA}} \quad (8)$$

where $F_{\text{pure } H_2}^{PSA}$ and $F_{H_2}^{PSA}$ represent the molar flow rates of the pure H_2 separated through the PSA and the H_2 fed into the PSA, respectively. The H_2 recovery ratio of 85% is adopted in the simulations for Processes 1, 2, 3, and 4.

In Processes 5, 6, 7, and 8, the useful products from the H_2-membrane SR include the H_2 and CO remaining in the reaction region ($F_{H_2}^R$ and F_{CO}^R) and the separated H_2 ($F_{H_2}^S$) in the permeate side. The fraction of H_2 recovered (on CO + H_2 basis) σ_F is defined by the following equation:

$$\sigma_F = \frac{F_{H_2}^S}{F_{H_2}^S + F_{CO}^R + F_{H_2}^R} \quad (9)$$

The fraction of H_2 recovered of 85% is adopted in the simulations of Processes 5, 6, 7, and 8.

The thermodynamic efficiency η_{Ex} is an important parameter for an integrated process.[22,23] The overall exergy efficiency for each process, defined as the exergy of the products over the total exergy input, is expressed as

$$\eta_{Ex} = \frac{Ex_{HPH_2} + Ex_{HPCO_2}}{Ex_{input} + W_{cp}^{CH_4}} \quad (10)$$

Table 8. Comparison of the Simulation Results with the Industrial Observed Values for the LWGS Reactor*

	Exit Gas Composition (%)	
	Industrial Data	Simulation
H_2	77.42	77.43
CO	0.43	0.34
CO_2	20.36	20.48
CH_4	1.79	1.75
Exit T (K)	505	502

*Adapted from González-Velasco et al.[20] Operation conditions: P, 17 × 10^5 Pa; input T, 480 K; steam feed flow, 0.208 mol/s; dry gas feed flow, 0.339 mol/s; composition of dry gas (%) of H_2/CO/CO_2/CH_4, 76.8/3.2/18.2/1.8.

Table 9. Mole Fractions of Different Species in the Streams of Major Units in Processes 1–4

Component	Mole Fraction						
	SR_{out}	$HWGS_{in}$	$HWGS_{out}$	$LWGS_{in}$	$LWGS_{out}$	PSA_{in}	Gas Mixture*
CH_4	0.01	0.01	0.01	0.01	0.01	0.01	0.03
H_2O	0.30	0.44	0.38	0.49	0.46	0.01	0.02
CO	0.11	0.09	0.03	0.02	9.E−4	2.E−3	0.01
H_2	0.53	0.42	0.48	0.40	0.43	0.79	0.35
CO_2	0.05	0.04	0.10	0.08	0.10	0.19	0.59

*Out of PSA.

Ex_{input} includes the exergy of the reactants, the exergy of the CH_4 fed into the furnace, and the exergy consumed for pure O_2 production. The standards for the exergy calculations are based on the data presented in Szargut et al.[21] W_{CP} represents the exergy consumption by the compressors, which is calculated based on the assumption that the thermodynamic efficiency of producing electricity from CH_4 is 50%. Ex_{HPH_2} and Ex_{HPCO_2} are the exergy of the pure H_2 and the captured CO_2 at 20 bar, respectively.

Results and Discussion

The simulated mole flow rates and the temperatures of the streams in each process are indicated as shown in Figures 1–8. For Processes 1–4, the mole fractions of different species of the streams feeding into and leaving the major units are listed in Table 9. And the mole fractions of different species in the rejected fuel gas mixture of the H_2-membrane SR are listed in Table 10.

Based on the simulation results, the input and output exergies of the eight processes are calculated and listed in Table 11. The thermodynamic efficiency, the amount of high pressure (HP) H_2 produced per mole of methane, the amount of CO_2 produced per mole of HP H_2, and the amount of CO_2 captured per mole of HP H_2 for the eight processes are listed in Table 11.

Among the eight processes, Processes 1 and 5 do not consider the CO_2 capture. The thermodynamic efficiency and the amount of HP H_2 (based on per mole of methane) of Process 5 is about 4 and 6% higher than those of Process 1, respectively. The advantage of Process 5 over Process 1 is mainly attributable to the application of an H_2-membrane. For the H_2-membrane steam reformer, the driving force for methane conversion not only comes from the energy provided by the CH_4 combustion in the furnace, but also comes from the removal of H_2 through the H_2-membrane. As indicated in Figures 1 and 5, to achieve a CH_4 conversion level of 95%, the temperature of the furnace of the conventional SR must reach 1178 K, which is >200 K higher than that of the H_2-membrane SR (about 960 K). To attain the higher operation temperature, more CH_4 is combusted in the furnace of the conventional SR, and thus the thermodynamic efficiency of Process 1 (about 70%) is lower than that of Process 5 (about 74%).

Based on Process 1, the alternative Processes 2, 3, and 4 consider CO_2 capture. In Process 2, because pure oxygen is used in the furnace and heater, the CO_2 in the flue gas can be captured after the water is condensed and separated. The input exergy of pure O_2, which reflects the exergy cost for the production of pure oxygen (the cumulative exergy consumption of pure O_2 is 237 kJ/mol),[21] accounts for roughly 15% of the total input exergy. With the same amount of HP H_2 produced per mole of CH_4 (2.66 mol_{H_2}/mol_{CH_4}), Process 2 has a thermodynamic efficiency drop of about 8% compared to that of Process 1.

In Processes 3 and 4, some separated H_2 is used as the fuel in the furnaces and in the heater. For Process 3, the exergy for pure O_2 production accounts for nearly 16% of the total input exergy. Because of the lower production of HP H_2 and the energy consumption for producing pure O_2, Process 3 has a thermodynamic efficiency drop of about 12% compared to that of Process 1. In Process 4, the steam reformer has an H_2-fired furnace; thus pure O_2 is used only in the furnace of the prereformer, so the input exergy of pure O_2 is lower than that of Processes 2 and 3. The thermodynamic efficiency of Process 4 is roughly 8% lower than that of Process 1. Processes 3 and 4 produce less HP H_2 (based on one mole of CH_4) and more CO_2 (based on one mole of HP H_2) compared to Process 1.

Based on Process 5, the alternative Processes 6, 7, and 8 take into account the CO_2 capture. For the comparable production of HP H_2 and CO_2 based on one mole of CH_4, Process 6 has a decrease of about 8% in thermodynamic efficiency compared to that of Process 5, which is mainly caused by the use of pure O_2. Process 7 has depreciations of roughly 10% in thermodynamic efficiency and roughly 2% in the production of HP H_2 (based on one mole of CH_4) compared to those of Process 5, because of the use of pure O_2 and the combustion of some separated H_2 in the furnace and the heater. In Process 8, the pure O_2 is used only in the prereformer, so the exergy cost for pure O_2 production is much lower than that of Processes 6 and 7. The thermodynamic efficiency of Process 8 is 68.3%, which is about 2% lower than that of Process 1 and about 6% lower than that of Process 5.

The H_2-membrane SR can achieve a given methane conversion with less fuel combusted in the furnace, so the processes with an H_2-membrane SR produce less CO_2 (based on one mole of HP H_2) than the processes with a conventional SR. Because of the advantages of an H_2-membrane SR and a lesser amount of pure O_2 used, Process 8 has the highest overall thermodynamic efficiency among the six processes with respect to CO_2 capture. Compared to Process 1, Process 8 has more hydrogen produced per amount of methane and a lower exergy lost.

Table 10. Mole Fractions of Different Species in the Rejected Gas Mixture in Processes 5–8

CH_4	H_2O	CO	H_2	CO_2
0.02	0.48	0.06	0.15	0.29

Table 11. Comparison of the Eight Processes*

Parameter	Process 1	2	3	4	5	6	7	8
E_x^{in} (kJ/s)								
Natural gas	1033.5	1034.3	853.2	853.2	977.3	983.2	853.2	853.2
Pure O_2	0	196.5	178.9	92.6	0	167.3	150.7	92.8
Water pump	1.5	1.6	1.6	1.7	0.1	0.1	0.1	0.1
H_2 compressor	68.6	68.6	53.2	53.0	64.6	64.6	58.4	58.4
CO_2 compressor	26.0	26.0	21.2	21.2	0	24.5	21.2	21.2
Air compressor	19.0	0	0	0	16.0	0	0	0
E_x^{out} (kJ/s)								
HP H_2	787.9	787.9	613.4	610.3	787.9	787.9	671.9	671.9
HP CO_2	0	34.2	28.2	28.2	0	32.4	28.2	28.2
Energy lost (kJ/s)	360.7	504.8	466.5	383.2	270.1	419.4	383.5	325.6
HP H_2 produced per mole CH_4 (mol_{H_2}/ mol_{CH_4})	2.66	2.66	2.52	2.50	2.82	2.80	2.76	2.76
CO_2 produced per mole HP H_2 (mol_{CO_2}/ mol_{H_2})	0.38	0.38	0.40	0.40	0.36	0.36	0.36	0.36
CO_2 captured per mole HP H_2 (mol CO_2 captured/ mol H_2)	0	0.38	0.40	0.40	0	0.36	0.36	0.36
Thermodynamic efficiency (%)	70.2	61.9	57.9	62.5	74.5	66.2	64.6	68.3

*E_x^{in}: exergy input; E_x^{out}: exergy output. The E_x^{in} of natural gas includes the CH_4 as the reactant and the CH_4 as the fuel.

Conclusions

The conventional steam-reforming process is taken as the basis for the alternative processes with respect to CO_2 capture. The captured CO_2 has a high purity and can be taken as a product. The adopted approaches include inputting pure oxygen instead of air into the furnaces and heaters, using some pure H_2 produced instead of CH_4 as the fuel, applying a prereformer to reduce the usage of pure oxygen, and applying an H_2-membrane to the steam reformer, combining the functions of producing and separating H_2 together. The processes were simulated based on the kinetic models of steam-reforming reactions and the permeation mechanism of hydrogen membrane. The processes were analyzed in terms of the thermodynamic efficiency, the production of high-pressure (HP) H_2 per mole of CH_4, the production of CO_2 per mole of HP H_2, and the CO_2 captured per mol of HP H_2. With the application of a prereformer to reduce the pure oxygen required and the application of an H_2-membrane steam reformer, Process 8 has the smallest efficiency penalty for CO_2 capture among the six processes with respect to CO_2 capture, even if some of the separated H_2 is combusted. So, for industrial application, we suggest that a process such as Process 8 can be considered as the potentially optimum method for CO_2 capture.

Acknowledgments

This work was supported by National Science Foundation of China Grants 20676014, 20676009, and 20576013.

Notation

a_r = cross-sectional area of reactor, m^2
a_{H_2} = H_2 membrane area per unit reactor length, m^2/m
a_v = area of particle per unit mass of catalyst, m^2/kg
a_w = area of the wall between reaction tube and the parallel furnace of the reformer, m^2/m
A_1 = area in Eq. 1
A_2 = area in Eq. 1
C_p = heat capacity, J/(mol·K)
$D_{e,f}$ = effective diffusion coefficient of species i in catalyst pellet, m^2/s
E_A = apparent activation energy of H_2 membrane, J/mol
$E_{a,k}$ = activation energy of reaction k, J/mol
E_x = exergy flow rate, J/s
F_t = total molar flow rate of i, mol/s
F_i = molar flow rate of i, mol/s
$F_{H_2}^S$ = production rate of separated H_2, mol/s
$F_{H_2}^R$ = molar flow rate of remaining H_2 in the rejected fuel gas from H_2 membrane reactor, mol/s
F_{CO}^R = molar flow rate of CO in the rejected fuel gas from H_2 membrane reactor, mol/s
F_l^{fh} = molar flow rate of combustible component l in the waste gas, mol/s
G_{H_2} = molar flow rate of H_2 in the nonreaction side, mol/s
G_j = molar flow rate of component j in the nonreaction side, mol/s
K_{eq} = equilibrium constant
k^{HWGS} = reaction rate constant of WGS reaction in HWGS reactor, $mol/(kg_{cat} \cdot s)$
k_0^{HWGS} = preexponential factor for reaction rate constant k^{HWGS}
K_i = adsorption constant of species i
K_i^0 = preexponential factor for adsorption parameters
k_k = reaction rate constant of reaction k
k_k^0 = preexponential factor for reaction rate, $mol/(kg_{cat} \cdot s)$
N_{H_2} = permeation rate through the H_2 membrane, $mol/(m^2 \cdot s)$
$N_i^{H_2}$ = component i permeation rate through H_2 membrane, $mol/(m^2 \cdot s)$
N_R = number of reactions
P_m = preexponential factor of the H_2 membrane, $mol \cdot m/(s \cdot m^2 \cdot bar^{0.5})$
$p_{s,i}$ = partial pressure of species i in catalyst particle, bar
p_i = partial pressure of species i in the gas phase, bar
$p_{H_2}^{high}$ = partial pressure of i in the reaction side, bar
$p_{H_2}^{low}$ = partial pressure of H_2 in the nonreaction side, bar
q = the heat flux between the reaction side and the nonreaction side, J/(s·m)
R = gas constant, J/(mol·K)
$-r_{CO}$ = the reaction rate in the WGS reactors, $mol/(kg_{cat} \cdot s)$
R_k = rate of reaction k in the main stream of the steam reformers, calculated with p_i, $mol/(kg_{cal} \cdot s)$
r_s = equivalent radius of the catalyst particle, m
$R_{s,k}$ = rate of reaction k inside the catalyst particle, calculated with $p_{s,i}$, $mol/(kg_{cat} \cdot s)$
T = absolute temperature, K
T_{fg} = temperature of rejected fuel gas, K
$T_{furnace}$ = temperature of parallel furnace of a steam reformer, K
T_{nr} = temperature in the nonreaction side of the membrane steam reformer, K
T_r = temperature in the reaction side of the steam reformers, K
$\bar{T}$ = average temperature of the membranes, K

T_0 = temperature of the environment, 298.15 K
U = heat transfer coefficient, J/(m^2·s·K)
W_{CP} = electric power used for compression, J/s
z = axial coordinate of the reactors, m

Greek letters

ε_B = void fraction of packing
δ_{H_2} = the thickness of the membrane layer, m
σ = fraction of H_2 recovered (on CO + H_2 basis)
η_{cp} = the exergy efficiency of compressor
η_{fhp} = efficiency of furnace or heater
η_{Ex} = overall exergy efficiency
η_k = effectiveness factor of reaction k
v_{ik} = stoichiometric coefficient of component i of reaction k
ρ_s = density of catalyst, kg/m^3
ξ = dimensionless pellet coordinate
ψ = the variable accounting the effect of P and diffusion into the catalytic slab
$\Delta H_{ads,i}$ = standard adsorption enthalpy of component i, kJ/mol
ΔH_{H_2} = the heat transferred by permeating H_2 from the reaction side to the nonreaction side, J/mol
$\Delta H_{heating}$ = the heat required by heating the reactants, J/s
ΔH_k = the heat of reaction k, J/mol
ΔH_l^{com} = the combustion heat of component l, J/mol
ΔH_{WGS} = the heat of WGS reaction, J/mol
$\Delta H_{T_{fs}}^{T_0}$ = the heat of fuel gas from T_{fg} to T_0, J/s
$\Delta H_{T_0}^{T_{end}}$ = the heat of flue gas from $T0$ to T_{end}, J/s

Literature Cited

1. Froment GF. Production of synthesis gas by steam- and CO_2-reforming of natural gas. *J Mol Catal A Chem*. 2000;163:147–156.
2. Chen Z, Prasad P, Yan Y, Elnashaie S. Simulation for steam reforming of natural gas with oxygen input in a novel membrane reformer. *Fuel Proc Technol*. 2003;83:235–252.
3. Simbeck DR. CO_2 capture and storage—The essential bridge to the hydrogen economy. *Energy*. 2004;29:1633–1641.
4. Dijkstra JW, Jansen D. Novel concepts for CO_2 capture. *Energy*. 2004;29:1249–1257.
5. Sircar S, Waldron WE, Rao MB, Anand M. Hydrogen production by hybrid SMR-PSA-SSF membrane system. *Sep Purif Technol*. 1999; 17:11–20.
6. Seo YS, Shirley A, Kolaczkowski ST. Evaluation of thermodynamically favorable operation conditions for production of hydrogen in three different reforming technologies. *J Power Source*. 2002;4724: 1–13.
7. Carcasci C, Facchini B. Comparison between two gas turbine solutions to increase combined power plant efficiency. *Energy Convers Manage*. 2000;41:757–773.
8. Xu J, Froment GF. Methane steam reforming, methanation and water gas shift: I. Intrinsic kinetics. *AIChE J*. 1989;35:88–96.
9. Elnashaie SSEH, Elshishini SS. Modeling, Simulation and Optimization of Industrial Fixed Bed Catalytic Reactors. London: Gordon & Breach; 1993.
10. Yu W, Ohmori T, Yamamoto T, Endo A, Nakaiwa M, Hayakawa T, Itoh N. Simulation of a porous ceramic membrane reactor for hydrogen production. *Int J Hydrogen Energy*. 2005;30:1071–1079.
11. Shu J, Grandjean BPA, Kaliaguine S. Methane steam reforming in asymmetric Pd and Pd-Ag/porous SS membrane reactor. *Appl Catal A Gen*. 1994;119:305–325.
12. Xu J, Froment GF. Methane steam reforming: II. Diffusional limitations and reactor simulation. *AIChE J*. 1989;35:97–103.
13. Moore WJ. Physical Chemistry. Englewood Cliffs, NJ: Prentice-Hall International; 1972.
14. Smith JM, Van Ness HC, Abbott MM. Introduction to Chemical Engineering Thermodynamics. 5th Edition. New York: McGraw-Hill; 1996.
15. Welty JR, Wilson RE, Wicks CE. Fundamentals of Momentum, Heat, and Mass Transfer. 2nd Edition. New York: Wiley; 1976.
16. De Smet CRH, de Croon MHJM, Berger RJ, Marin GB, Schouten JC. Design of adiabatic fixed-bed reactors for the partial oxidation of methane to synthesis gas. Application to production of methanol and hydrogen-for-fuel-cells. *Chem Eng Sci*. 2001;56:4849–4861.
17. Basile A, Paturzo L, Lagana F. The partial oxidation of methane to syngas in a palladium membrane reactor: Simulation and experimental studies. *Catal Today*. 2001;67:65–75.
18. Bohlbro H. An Investigation on the Kinetics of the Conversion of Carbon Monoxide with Water Vapor over Iron Oxide-based Catalysts. 2nd Edition. Copenhagen, Denmark: Gjellerup; 1969.
19. Amadeo NE, Laborde MA. Hydrogen production from the low-temperature water-gas-shift reaction: Kinetics and simulation of the industrial reactor. *Int J Hydrogen Energy*. 1995;20:949–956.
20. González-Velasco JR, Gutiérrez-Ortiz MA, González-Marcos JA, Amadeo NE, Laborde MA, Paz M. Optimal inlet temperature trajectories for adiabatic packed reactors with catalyst decay. *Chem Eng Sci*. 1992;47:1495–1507.
21. Szargut J, Morris DR, Steward FR. Exergy Analysis of Thermal, Chemical and Metallurgical Processes. New York: Hemisphere; 1998.
22. Kjelstrup S, De Swaan Arons J. Denbigh revisited: Reducing lost work in chemical processes. *Chem Eng Sci*. 1995;50:1551–1560.
23. Rosen MA, Scott DS. Entropy production and exergy destruction: Part II—Illustrative technologies. *Int J Hydrogen Energy*. 2003;28: 1315–1323.

Manuscript received Mar. 28, 2006, and revision received Oct. 12, 2006.